The FASEB Journal

RESEARCH ARTICLE OPEN ACCESS

The RNA-Binding Proteins MCPIP2 and IGF2BP1 Competitively Modulate Breast Tumor Angiogenesis by Antagonizing VEGFA mRNA Stability and Expression

Wenbao Lu | Hongwei Li | Xueting Liu | Ailing Li | Ruijuan Xiu

Institute of Microcirculation, Chinese Academy of Medical Sciences & Peking Union Medical College, Beijing, China

Correspondence: Wenbao Lu (luwenbao_217@imc.pumc.edu.cn)

Received: 16 February 2025 | **Revised:** 5 April 2025 | **Accepted:** 22 April 2025

Funding: This work was supported by MOST | National Natural Science Foundation of China (NSFC) (Grant 82372619).

Keywords: breast cancer | IGF2BP1 | MCPIP2 | RNA-binding protein | tumor angiogenesis

ABSTRACT

Tumor angiogenesis is essential for further growth and metastasis of solid tumors. However, the mechanisms underlying angiogenesis-related gene expression have yet to be clarified. Here, we discovered RNA-binding proteins monocyte chemotactic protein-induced protein 2 (MCPIP2) and insulin-like growth factor 2 mRNA-binding protein 1 (IGF2BP1) function as a pair of antagonists that modulate breast tumor angiogenesis by competitively regulating mRNA stability of proangiogenic gene transcripts, including *vascular endothelial growth factor A* (*VEGFA*), *Erb-B2 receptor tyrosine kinase 2* (*ERBB2*), *interleukin-8* (*IL8*), *C-X-C motif chemokine ligand 1* (*CXCL1*), and *ephrin A1* (*EFNA1*). Mechanistically, MCPIP2 physically interacted with the stem–loop structures in the 3′-untranslated region of proangiogenic transcripts through its RNase domain to destabilize their mRNAs. Ribosomal proteins might be required for MCPIP2-mediated destabilization of proangiogenic mRNAs. On the other hand, IGF2BP1 can stabilize the proangiogenic mRNAs by binding to the common RNA stem–loop structures. Furthermore, we found that MCPIP2 expression in human breast tumors was repressed, whereas IGF2BP1 expression increased. Lower MCPIP2 expression and higher IGF2BP1 expression in human breast tumors were significantly associated with poor survival of breast cancer patients, respectively. Notably, there was a reversed correlation relationship between MCPIP2, IGF2BP1 expression, and proangiogenic gene expression in human breast tumor samples. Collectively, our results elucidate a novel mechanism by which MCPIP2 and IGF2BP1 competitively modulate the expression of proangiogenic transcripts, which provides new insights into antiangiogenic therapy of breast cancer.

1 | Introduction

Breast cancer has become the most common cancer among women worldwide. Although the 5-year survival rate of patients has increased due to early diagnosis and surgical treatment, the mechanism of tumorigenesis and progression is still unclear. Tumor angiogenesis is a key step for further growth and distant metastasis of breast tumors. The initiation of tumor

Abbreviations: 3′UTR, 3′ untranslated region; ActD, actinomycin D; ARE, AU-rich element; ATCC, American Type Culture Collection; C4BPA, C4b-binding protein alpha chain; CELF2, CUGBP Elav-like family member 2; CXCL1, C-X-C motif chemokine ligand 1; DMEM, Dulbecco's modified Eagle's medium; DRB, 5, 6-dichlorobenzimidazole riboside; EFNA1, ephrin A1; ELAVL2, ELAV-like neuronal protein 1; ELISA, enzyme-linked immunosorbent assay; ERBB2, Erb-B2 receptor tyrosine kinase 2; HSPB1, heat shock protein beta-1; IGF2BP1, insulin-like growth factor 2 mRNA-binding protein 1; IL8, interleukin-8; MCPIP2, monocyte chemotactic protein-induced protein 2; MEF, - mouse embryonic fibroblast; MS, mass spectrometry; RBM47, RNA-binding protein 47; RBP, RNA-binding protein; RIP-ChIP, RNA immunoprecipitation-chromatin immunoprecipitation; RPC, RNA-protein complex; RPS3A, ribosomal protein s3a; SAMD4A, sterile alpha motif domain-containing protein 4A; shRNA, short hairpin RNA; SL, stem–loop; VEGFA, vascular endothelial growth factor A; ZF, zinc finger.

angiogenesis is determined by various angiogenic factors that are produced mainly by tumor cells [1]. Angiogenesis-associated genes can be divided into proangiogenic genes, such as *Erb-B2 receptor tyrosine kinase 2* (*ERBB2*) [2], *vascular endothelial growth factor A* (*VEGFA*) [3], *interleukin-8* (*IL8*) [4], *C-X-C motif chemokine ligand 1* (*CXCL1*) [5] and *ephrin A1* (*EFNA1*) [6] and antiangiogenic genes, such as *collagen type XV alpha 1 chain* (*COL15A1*) [7], *tissue inhibitor of matrix metalloprotease 1* (*TIMP1*) [8], *serpin family F member 1* (*SERPINF1*) [9], *C-X-C motif chemokine ligand 11* (*CXCL11*) [10], and *angiopoietin-like protein 1* (*ANGPTL1*) [11]. An imbalance between these genes can elicit pathogenic angiogenesis, including tumor angiogenesis [12]. Therefore, reversing the imbalanced gene expression of angiogenesis-associated genes within tumor cells could play a role in the regulation of tumor angiogenesis. However, how angiogenesis genes are regulated in tumor cells, especially by RNA-binding proteins (RBPs) at the posttranscriptional level, remains unclear.

MCPIP2, a Cys-Cys-Cys-His-type zinc-finger RNA-binding protein encoded by the *Zc3h12b* gene, was also named Regnase-2 according to its endoribonuclease activity [13]. Initially, it was identified as a member of the MCP-induced protein family [14]. MCPIP2 can inhibit the expression of proinflammatory cytokines, such as IL6 and interleukin-1β (IL1β), by decaying mRNA [15, 16]. Therefore, MCPIP2 can act as a brake against excessive autoinflammation. MCPIP2 has an RNase domain and can bind to a structured RNA motif but not linear RNA sequences [17]. To date, a few studies have shown that MCPIP2 is involved in the progression of several human cancers. MCPIP2 is involved in immune escape in colon cancer cells [18] and regulates the tumorigenesis and progression of ovarian cancer [19]. In addition, MCPIP2 can suppress glioblastoma cell proliferation [20], and its expression level may predict the prognosis of glioma patients [21]. However, it remains unknown whether MCPIP2 plays a role in breast cancer progression and tumor angiogenesis regulation.

In this study, we demonstrated the expression patterns of all RBPs (1756 RBPs) in breast cancer and revealed that MCPIP2 acts as a potent tumor suppressor by inhibiting tumor angiogenesis through specifically suppressing the expression of proangiogenic gene transcripts, including *ERBB2*, *VEGFs*, *IL8*, *CXCL1*, and *EFNA1*. The expression of MCPIP2 is reduced in breast tumors, and low MCPIP2 mRNA expression levels are correlated with poor survival in breast cancer patients. Ectopic expression of MCPIP2 downregulated proangiogenic gene expression and inhibited breast tumor-induced angiogenesis, whereas knockdown of MCPIP2 enhanced tumor angiogenesis. MCPIP2 destabilizes proangiogenic mRNAs by targeting conserved stem–loop structures in 3′-untranslated regions (3′UTRs) via the RNase domain. Moreover, we found for the first time that ribosomal protein s3a (RPS3A) can interact with MCPIP2 and attenuate its mRNA degradation in breast tumor cells. Interestingly, insulin-like growth factor 2 mRNA-binding protein 1 (IGF2BP1), another RBP [22, 23], was shown to antagonize MCPIP2-mediated inhibition of breast tumor angiogenesis by stabilizing proangiogenic mRNAs. These results suggest that MCPIP2 and IGF2BP1 are potent antagonists involved in negatively and positively regulating the angiogenesis pathway in breast tumors, respectively, by competing to regulate proangiogenic gene expression.

2 | Materials and Methods

2.1 | Bioinformatic Analysis of RBP Expression in Human Breast Tumor Datasets

Human breast tumor datasets were downloaded from the TCGA data portal (https://tcga-data.nci.nih.gov/tcga/). The expression matrix was selected only from the primary tumors and their adjacent health tissues. The known 1756 genes coding for RNA-binding proteins were analyzed. The limma package of R studio (version 4.0.0) was used for differential analysis of target genes (cutoff:|log2FC| > 1 & FDR < 0.05).

2.2 | Cell Lines and Plasmids

Human breast cancer cell lines (MDA-MB-468, MDA-MB-231, MCF7, and T47D) and human normal mammary epithelial cell lines (MCF-10A and, MCF-12A) were obtained from the American Type Culture Collection (ATCC; Manassas, VA, USA) and cultured in DMEM or PRM1640 medium with 10% FBS plus 1% Peni/Stro, respectively. Immortalized human umbilical vein endothelial cells (HUVEC), HEK293, and HEK293T cells were obtained from the National Infrastructure of Cell Line Resource (Beijing, China). The human full-length MCPIP2 coding sequence (NM_001010888.3) and IGF2BP1 coding sequence (NM_006546.4) were synthesized, sequenced, and inserted into the pEGFP-N1 vector at NgeI/SacII and NheI/SacI sites, respectively. MCPIP2 serial deletion plasmids were generated by inserting the PCR-amplified fragments into the pEGFP-N1 vector at NgeI and SacII sites. The luciferase reporters were constructed by inserting the full-length 3′UTRs of human *ERBB2*, *VEGFA*, *IL8*, *EFNA1*, *CXCL1*, *COL15A1*, *SERPINF1*, *TIMP1*, and *CXCL11* into the pGL3 control vector (Promega; Madison, WI, USA) between Xba I and Fse I sites, respectively. For stem–loop deletion reporters, point-mutated and truncated *ERBB2*-3′UTR (Δstem–loop) and *VEGFA*-3′UTR (Δstem–loop) were amplified, sequenced, and inserted into the pGL3 control vector using the Phusion Site-Directed Mutagenesis Kit (Thermo Scientific; Waltham, MA, USA).

2.3 | Antibodies and Reagents

Polyclonal rabbit anti-MCPIP2 (PA5-20927), anti-IGF2BP1 (PA5-23968), anti-GFP (A-11122), and anti-CD31 (PA1-37326) were from Thermo Scientific (Waltham, MA, USA). Isotype normal rabbit IgG (ab37415) was from Abcam (Cambridge, UK). Polyclonal rabbit anti-ERBB2 (18299-1-AP), anti-VEGFA (19003-1-AP), anti-VEGFC (22601-1-AP), anti-PDGFC (55076-1-AP), anti-PDGFD (14075-1-AP), anti-RPS3A (14123) antibodies were from Proteintech Co (Cook County, IL, USA). Rabbit IL8 (A2541) and mouse β-actin (AC004) antibodies were from ABclonal Company (Wuhan, China). G418 (G8168), puromycin (P8833), actinomycin D (ActD, A1410), and 5, 6-dichlorobenzimidazole 1-β-D-ribofuranoside (DRB, D1916) were from Sigma-Aldrich (St. Louis, USA). Protein A/G PLUS-Agarose beads were from Santa Cruz Biotechnology (San Diego, CA, USA). GFP-coated beads (gta-20) were from ChromoTek (Munich, Germany). Dynabeads M-280 streptavidin (11205D) were from Invitrogen (Grand Island, USA).

2.4 | RNA Isolation and qRT-PCR

Total RNA was extracted with TRIzol from tissues or cultured cells and reverse transcribed to cDNA for qPCR using SYBR green Fast Master Mix (#04913850001; Roche, Basel, Switzerland). Gene expression levels were based on the ΔΔCt method and normalized to GAPDH.

2.5 | Western Blotting

Cell or tissue samples were collected and lysed with a modified RIPA buffer containing PMSF and protease inhibitor cocktail (#04693159001, Roche; Basel, Switzerland). Protein concentration was measured by BCA method. Equal amounts of protein lysates were subjected to electrophoresis by SDS-PAGE and transferred onto a polyvinylidene membrane. The membrane was then blocked with 5% fat-free milk and incubated with primary antibody (dilution: 1:1000 in 5% fat-free milk) overnight at 4°C. The band was detected with HRP-conjugated secondary antibodies (dilution: 1:5000 in 5% fat-free milk) using ECL chemiluminescent detection method (#34077, Pierce; Rockford, IL, USA).

2.6 | Kyoto Encyclopedia of Genes and Genomes (KEGG) Pathway and Gene Ontology Analysis

The commonly up- and downregulated mRNAs by MCPIP2 or IGF2BP1 in breast tumor cells were classified using the Venn diagram. KEGG pathway and GO analyses of differentially expressed genes were done using DAVID (http://david.abcc.nifcrf.gov/).

2.7 | RNA Immunoprecipitation (RIP)

Total protein extracts were obtained from MDA-MB-468 cells and precleared with IgG, followed by incubation with anti-MCPIP2 antibody or isotype IgG at 4°C for 4 h, respectively. RNA-protein complexes were immunoprecipitated with protein A/G agarose beads. The pulled down RNAs were extracted from the beads and reverse transcribed to cDNA for qPCR detection. MDA-MB-468 cells expressing MCPIP2-GFP or an empty vector were lysed and whole-cell lysates were precleared with IgG and then incubated with GFP-trap beads (ChromoTek, Munich, Germany) for 4 h at 4°C. The RNA-protein complexes were pulled down by GFP-trap beads and RNA extracted with TRIzol, followed by testing with RT-PCR.

2.8 | Wound Healing Assay

Human umbilical vein endothelial cells (HUVECs) were seeded in a 96-well plate (1×10^4 cells/well) and incubated at 37°C. After the cells formed a monolayer, a scratch in the cell monolayer was created using a pipette tip, and the cells were incubated for 24 h. The images of the scratch were acquired using a microscope (Carl Zeiss Microimaging, Gottingen, Germany), and the open area of the wound was quantified using ImageJ software.

2.9 | Tube Formation Assay

96-well plates were placed on ice and coated with 50 μL prethawed Matrigel (#356234, BD Biosciences, NJ, USA) per well and incubated for 1 h in a 37°C incubator. 1×10^4 HUVECs were seeded on the gel with 100 μL of tumor conditioned medium (CM) concentrated using an ultrafiltration device (Millipore, Bedford, MA, USA). After 12 h, the tube formation was captured using a microscope (Carl Zeiss Microimaging, Gottingen, Germany), and the number of branch points was quantified.

2.10 | Luciferase Reporter Assays

Luciferase assay was performed as described previously. pGL3 luciferase reporter constructs containing full-length or segments of the 3′UTR of different genes were transfected into HEK293 cells along with MCPIP2, IGF2BP1, truncations, and GFP-control constructs, respectively. All transfections were conducted in triplicate and repeated at least three times. The luciferase activity was measured 36 h after transfection using a Dual-Luciferase Reporter Assay System (Promega, Madison, WI, USA).

2.11 | Immunocytochemistry

MDA-MB-468 cells were fixed in 4% paraformaldehyde in PBS for 15 min and then permeabilized in 0.5% Triton X-100 in PBS for 10 min. Cells were washed three times and blocked in 1.0% BSA for 30 min at room temperature. Primary antibodies to MCPIP2 and RPS3A were used for staining in combination with secondary antibodies conjugated to FITC or Alexa Fluor 555 (Invitrogen, Grand Island, USA). DAPI was used for nucleus staining. Images were captured on a Zeiss microscope.

2.12 | RNA Sequencing

RNA sequencing was completed by Allwegene Technology Inc., Beijing, with the PE150 sequencing strategy using an Illumina second-generation high-throughput sequencing platform. The reads with inferior quality or adapters were filtered. Clean read data were processed using Tophat2 and Cufflinks software to complete the alignment of transcriptomes. Genes not expressed in any sample were excluded from further analysis. Differentially expressed genes and transcripts were then filtered for false discovery rate (FDR)-adjusted p values less than or equal to 0.05. Detailed RNA-seq data are shown in Tables S1 and S4.

2.13 | Protein Pull-Down and Mass Spectrometry

Immunoprecipitation was carried out using GFP-Trap Agarose (gta-20, ChromoTek, Munich, Germany) in MDA-MB-468/GFP cells and MDA-MB-468/GFP-MCPIP2 cells, according to the manufacturer's instructions. Briefly, cells were washed and lysed in NP-40 buffer. Whole cell lysates were centrifuged

to separate the pellet from the soluble fraction. GFP-Trap agarose beads were incubated with the soluble lysates by rotating at 4°C for 2 h. Then, the pulled-down proteins were separated by running SDS-PAGE and silver staining and identified by high-resolution mass spectrometry carried out by Beijing Qinglian Biotech Co. Ltd. (Beijing, China) with the RIGOL L-3000 HPLC System (RIGOL, Beijing, China). The raw data were searched against the *homo sapiens* database by Proteome Discoverer 2.4 with Sequest HT (Thermo Fisher Scientific, MA, USA). All proteins were summarized in Table S2.

2.14 | RNA Pull-Down and Mass Spectrometry

Aliquots of 3′-biotin-labeled different RNA probes (with stem-loop or without stem-loop) were used for RNA pull-down experiments. Total protein extracts were obtained from MDA-MB-468 cells with NP-40 buffer and were precleared with streptavidin-coated Dynabeads (M-280, Invitrogen, MA, USA) and then incubated with RNA probes and Dynabeads for 2 h at 4°C. Beads were washed six times and then boiled in SDS-PAGE sample buffer. The RNA-bound proteins were eluted and resolved by SDS-PAGE followed by silver staining. The unique separated bands were excised and in-gel digested with trypsin for mass spectrometry (LC–MS) analysis by Beijing Qinglian Biotech Co. Ltd. (Beijing, China) with RIGOL L-3000 HPLC System (RIGOL, Beijing, China). The raw data were searched against the *homo sapiens* database by the Proteome Discoverer 2.4 with Sequest HT (Thermo). All proteins were summarized in Table S3.

2.15 | mRNA Stability

Cells were added actinomycin D (ActD, 5 μg/mL) and 5, 6-dichlorobenzimidazole riboside (DRB, 5 μg/mL) to block *de novo* RNA synthesis. Total RNA was collected at indicated time points, and the relative mRNA level was analyzed by qRT-PCR. The half-life of mRNA was determined by comparing the levels of mRNA before adding ActD and DRB. All primers are provided in Table S5.

2.16 | RNA Immunoprecipitation-Chromatin Immunoprecipitation (RIP-ChIP)

MCPIP2/GFP fusion protein was expressed in MDA-MB-468 cells for 36 h. Then, cells were cross-linked for 10 min by the addition of formaldehyde (1% v/v). Glycine (G8790; Sigma-Aldrich, St. Louis, USA) was used to stop crosslinking (125 mM). Cells were washed with cold PBS, resuspended in 500 μL of polysome lysis buffer, and placed on ice for 5 min. Cell lysates were collected by centrifugation at 10 000 *g* for 10 min at 4°C and re-suspended in 500 μL of polysome lysis buffer. Then, the lysates were sonicated and pre-cleared with rabbit IgG to remove non-specific background. Pre-cleared lysates were used for IP with GFP-coated beads or rabbit IgG-coated beads at 4°C for 4 h. After pull-down, 100 μL supernatants were taken out for Input. Each immune complex was washed at least five times with ice-cold NT2 buffer. RNA was isolated with Trizol reagent and re-suspended in 50 μL of RNase-free water, followed by DNase I (EN0521, Thermo Scientific; Waltham, MA, USA) treatment and further detection.

2.17 | ELISA Assay

Human CXCL1 and VEGFA levels of conditioned mediums (CMs) from different tumor cells were assessed with commercially available ELISA kits (RAB0116, RAB0507, Sigma, MO, USA) according to the manufacturer's instructions.

2.18 | RNA-EMSA (Electrophoretic Mobility Shift Assay)

20 fmol of the 3′-end biotin-labeled probes were incubated with 15 μg of total cell lysates containing MCPIP2/GFP or IGF2BP1/GFP fusion protein for 30 min at room temperature with 20 μL of binding buffer. RNA-protein complexes were resolved by 6% non-denaturing polyacrylamide gel electrophoresis, and the gel was transferred onto a nylon membrane and UV-cross linked. The membrane was then subjected to detection by chemiluminescent EMSA kit (Pierce, IL, USA) following the manufacturer's protocol.

2.19 | shRNA Lentivirus and Adenovirus

Two lentiviral shRNAs (TRCN0000172544; TRCN0000172337) targeting human MCPIP2 mRNA, two lentiviral shRNAs (TRCN0000074711; TRCN0000289165) targeting human RPS3A mRNA, and two lentiviral shRNAs targeting human CXCL1 (TRCN0000057939) and VEGFA (TRCN0000003343) were purchased from Merck (New Jersey, USA). A scramble control shRNA was used as a control. Lentiviral particles were packaged in HEK293T cells by cotransfecting shRNA-pLKO.1, pCMV-dR8.2, and pMD2.G constructs. After two rounds of infection, the target cells were selected with puromycin (1.0 μg/mL) for 2 weeks. MCPIP2/GFP-expressing adenovirus, IGF2BP1/GFP-expressing adenovirus, or GFP-expressing control adenovirus were packaged by GeneChem Company (Shanghai, China).

2.20 | Animal Study

Female BALB/c nude mice (6-weeks old) were from the Institute of Laboratory Animal Science, Chinese Academy of Medical Sciences (CAMS) and Peking Union Medical College (PUMC). MDA-MB-468/MCPIP2-GFP (5×10^6/100 μL PBS), MCF7/MCPIP2-GFP (3×10^6/100 μL PBS), MDA-MB-468/IGF2BP1-GFP (5×10^6/100 μL PBS), and their control cells were injected subcutaneously into the fat pad of the mammary gland of nude mice, respectively. For tumor treatment with adenovirus, MDA-MB-468 cells (5×10^6/100 μL PBS) were injected into nude mice according to the above methods. When tumors reached ~5 mm in diameter, MCPIP2/GFP-expressing adenoviruses or GFP-expressing control adenoviruses (from GeneChem, Shanghai) were injected into the tumors (10^{10} pfu/tumor each time). Tumor size was measured by the

formula length × width × height (mm^3). All experimental procedures were approved by the Experimental Animal Care and Ethics Committee of the Institute of Microcirculation, CAMS & PUMC.

2.21 | Immunohistochemistry (IHC) and Hematoxylin and Eosin (H&E) Staining

Xenograft tissues or human breast tumor and surrounding healthy tissues were subjected to IHC to detect the expression of the interested proteins using the indicated antibodies. Mouse lung tissues were treated with H&E for staining. The Zeiss Imaging System was used to visualize the stained sections.

2.22 | Tumor Tissue Samples

A total of 18 human breast tumor samples and their matched surrounding 'healthy' tissues were obtained previously [24]. The tumors have mixture of molecular subtypes, including eight luminal A, three luminal B, and four triple negative breast tumors. The subtypes of the rest three tumors are unknown. Among these tumors, seven samples were evaluated as having higher MCPIP2 expression (MCPIP2-positive), and eleven samples showed lower MCPIP2 expression (MCPIP2-negative) according to IHC scoring. Nine samples were evaluated as having higher IGF2BP1 expression (IGF2BP1-positive), and eight samples showed lower IGF2BP1 expression (IGF2BP1-negative). The study was conducted in accordance with the Declaration of Helsinki, and the experimental protocols were approved by the Medical Ethics Committee of the Institute of Microcirculation, CAMS & PUMC.

2.23 | Sequence Alignments and Stem-Loop Structure Prediction

For 3′UTR stem-loop structure sequence conservation analysis of *ERBB2*, *VEGFA*, *IL8*, *EFNA1*, and *CXCL1*, the 3′UTR sequences were extracted for different species from the National Center for Biotechnology Information (NCBI) database: *ERBB2* 3′UTR: human (*Homo sapiens*; accession number NM_004448.4), chimpanzee (*Pan troglodytes*; XM_054671555.1), mouse (*Mus musculus*; NM_001003817.1), rat (*Rattus*; NM_017003.2); *VEGFA* 3′UTR: human (*Homo sapiens*; NM_003376.6), chimpanzee (*Pan troglodytes*; XM_016955592.3), mouse (*Mus musculus*; NM_001287056.1), rat (*Rattus*; NM_031836.3); *IL8* 3′UTR: human (*Homo sapiens*; NM_000584.3), chimpanzee (*Pan troglodytes*; XM_001156432.5), *Microcebus murinus* (*Microcebus murinus*; XM_012744803.1); *EFNA1* 3′UTR: human (*Homo sapiens*; NM_004428.3), chimpanzee (*Pan troglodytes*; XM_003308425.4), mouse (*Mus musculus*; NM_001162425.1), rat (*Rattus*; NM_053599.3), *CXCL1* 3′UTR: human (*Homo sapiens*; NM_001511.4), chimpanzee (*Pan troglodytes*; XM_001156094.8), mouse (*Mus musculus*; NM_008176.3), and rat (*Rattus*; NM_030845.2). Stem-loop sequence conservation analysis was performed using DNAMAN software. The stem-loop structure was predicted through RNAfold web server (http://rna.tbi.univie.ac.at/).

2.24 | Statistical Analysis

Data in bar graphs represent mean ± SD of at least three biological repeats. Statistical analysis was performed using Student's *t*-test by comparing treatment versus vehicle control or otherwise as indicated. Comparisons between groups were analyzed by Prism 9 and made by *t*-test. Spearman correlation analysis was used to evaluate the relationship between different gene expression levels. $p < 0.05$ was considered to be statistically significant.

3 | Results

3.1 | MCPIP2 Is Reduced in Human Breast Tumors and Positively Correlated With Patient Survival

We first analyzed the expression of 1756 RBP mRNAs in breast cancer patients by surveying the public data sets from The Cancer Genome Atlas (TCGA) [25, 26] and found that MCPIP2 had lower expression and ranked among the candidates with the lowest expression of all the RBPs (Figure 1A). MCPIP2 mRNA expression in breast tumors was significantly lower than that in normal tissues according to TCGA data (Figures 1B,C and S1A) and our collected tumor samples (Figure 1D). A reduction in MCPIP2 mRNA expression was also observed in human breast tumor cells compared with normal mammary gland epithelial cells (Figure S1B). Furthermore, *MCPIP2* expression is also lower in different subtypes of breast cancers (Figure 1E,F). Interestingly, the *MCPIP2* expression level gradually decreased with increasing breast cancer stage (Figure 1G), suggesting that *MCPIP2* expression might be associated with the progression of breast cancer. We also demonstrated that MCPIP2 protein expression was lower in human breast tumor samples (Figure 1H) and breast tumor cells (Figure 1I). Immunohistochemistry (IHC) staining of breast tumor samples further confirmed the lower expression of MCPIP2 in breast tumors (Figure 1J). Additionally, Kaplan–Meier plots showed that breast cancer patients with lower *MCPIP2* levels tended to die more often than patients whose tumors had higher levels of *MCPIP2* (Figures 1K–N and S1C). Although no significant correlation was detected between *MCPIP2* expression and patient survival in the basal and HER2+ subtypes, a similar trend suggested that patients with lower *MCPIP2* expression exhibited poorer survival (Figure S1D,E). Overall, these findings clearly demonstrated that MCPIP2 expression was reduced in breast tumors and strongly associated with patient survival.

3.2 | MCPIP2 Regulates the Expression of Angiogenesis-Related Genes in Breast Cancer Cells and Inhibits Breast Tumor-Induced Angiogenesis

To determine the target genes and signaling pathways regulated by MCPIP2 at the whole-transcriptome level, RNA sequencing was performed using MCPIP2-overexpressing MDA-MB-468 and MCF7 cells (Figure S2A). A total of 4950 genes were commonly downregulated, and 3288 genes were commonly upregulated in these two breast tumor cells (Figure S2B and Table S1). Gene

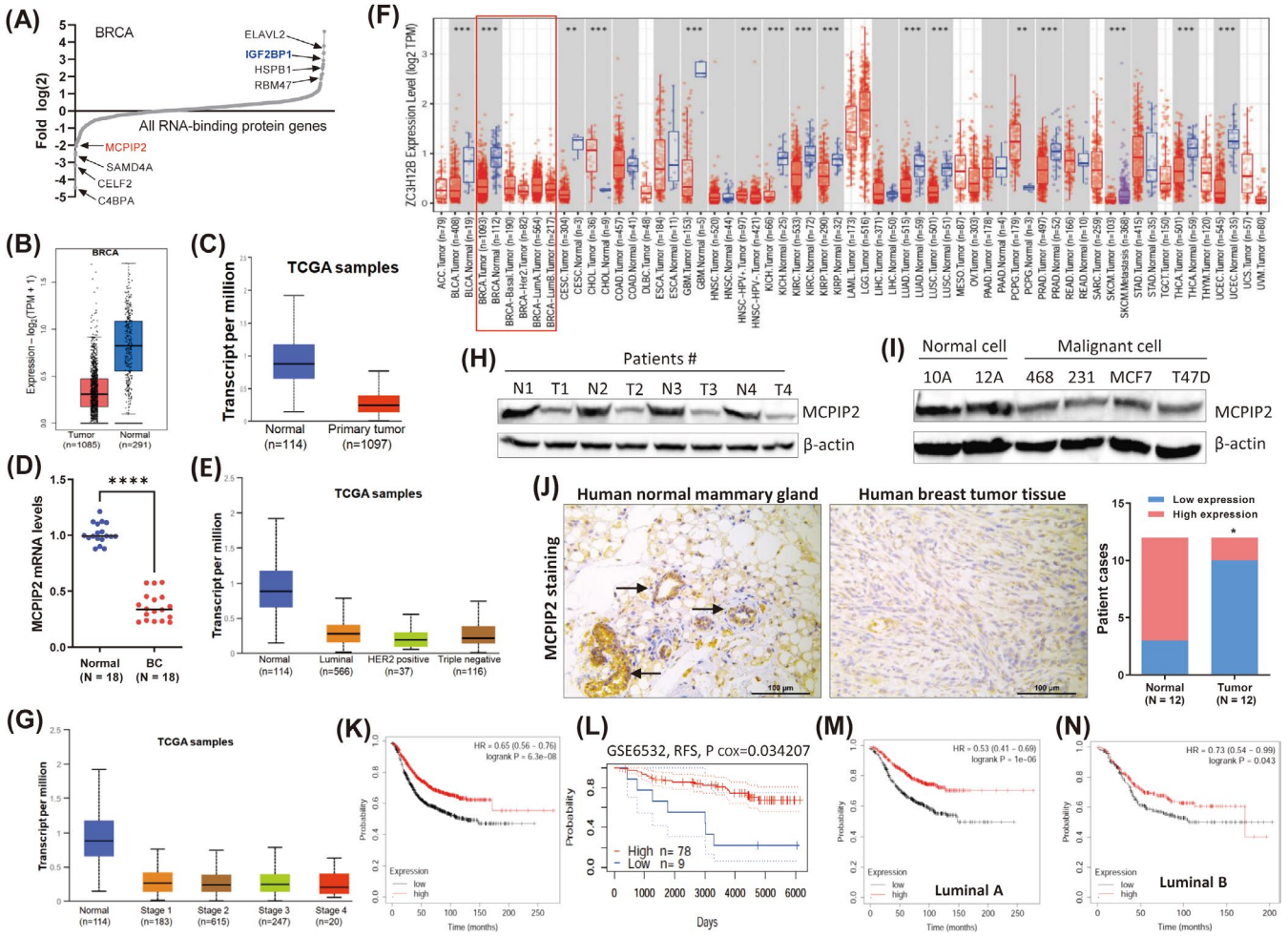

FIGURE 1 | MCPIP2 is reduced in human breast tumors and positively correlated with patient survival. (A) Expression profiling of 1756 RNA-binding protein genes in human breast tumors using the TCGA database. (B) *MCPIP2* expression in human breast tumors and normal breast tissues through GEPIA2 (http://gepia2.cancer-pku.cn/#analysis). (C) Expression of *MCPIP2* in human primary breast tumors and normal tissues (http://ualcan.path.uab.edu/analysis-prot.html). (D) MCPIP2 mRNA expression was measured by qRT-PCR in human breast tumor specimens ($n = 18$) compared with surrounding "normal" breast tissue ($n = 18$). (E) Expression level of *MCPIP2* between different subtypes of breast cancers was analyzed (http://ualcan.path.uab.edu/analysis-prot.html). (F) Expression of *MCPIP2* in tumor and adjacent normal tissues across various cancer types in TCGA cohorts was analyzed through TIMER2.0 (timer.cistrome.org). (G) Expression levels of MCPIP2 were analyzed by the main pathological stages of breast cancers (http://ualcan.path.uab.edu/analysis-prot.html). (H, I) MCPIP2 protein levels were measured by western blot in human breast tumor tissues (H) and breast tumor cell lines (I). (J) Representative images of MCPIP2 IHC stating in normal mammary gland tissues and breast tumor tissues were shown (left). Scale bar, 100 μm. IHC scores of matched breast tumor and normal tissues ($n = 12$) were evaluated based on MCPIP2 staining (right). (K, L) Kaplan–Meier Relapse-Free Survival analyses of breast cancer patients with low and high MCPIP2 transcripts were performed using Kaplan–Meier Plotter (K) (kmplot.com) and PrognoScan (L) (PrognoScan: A new database for meta-analysis of the prognostic value of genes. (kyutech.ac.jp)). (M, N) Relapse-Free Survival curves of luminal A (M) and luminal B (N) subtypes breast cancer patients with low and high MCPIP2 transcripts. Data are presented as mean ± SD; $^{*}p < 0.05$, $^{***}p < 0.0001$, $^{****}p < 0.00001$ in unpaired *t*-test.

ontology (GO) analysis revealed that the regulated genes were strongly enriched for transcripts associated with 'angiogenesis', 'regulation of vascular permeability', and 'regulation of mRNA stability' (Figure 2A), suggesting that MCPIP2 might be involved in regulating angiogenesis-related gene expression in breast tumor cells. Indeed, a series of proangiogenic genes, including *VEGFA*, *ERBB2*, *IL8*, *CXCL1*, and *EFNA1*, were downregulated by MCPIP2, and many antiangiogenic genes, such as *COL15A1*, *TIMP1*, *SERPINF1*, *CXCL11*, and *ANGPTL1*, were upregulated (Figure 2B,C). qRT-PCR confirmed that MCPIP2 downregulated proangiogenic mRNA expression (Figure 2D) and increased antiangiogenic gene expression (Figure S2C) in breast tumor cells. Moreover, we also found that the protein expression of the proangiogenic genes VEGFA/C, ERBB2, PDGFC/D (platelet-derived growth factor C/D), and IL8 was downregulated by MCPIP2 in breast tumor cells, although IL8 could not be detected by western blot in MCF7 cells (Figure 2E). The ELISA results also indicated that MCPIP2 could reduce the levels of VEGFA and CXCL1 proteins in tumor CMs (Figure 2F). These results suggested that MCPIP2 may play a role in regulating breast tumor-induced angiogenesis. To confirm this, we first examined the effect of CMs from MCPIP2-overexpressing breast tumor cells on human umbilical vein endothelial cell (HUVEC) migration and tube formation in vitro. CMs harvested from MCPIP2-overexpressing breast tumor cells significantly inhibited endothelial cell migration (Figures 2G and S2D) and tube

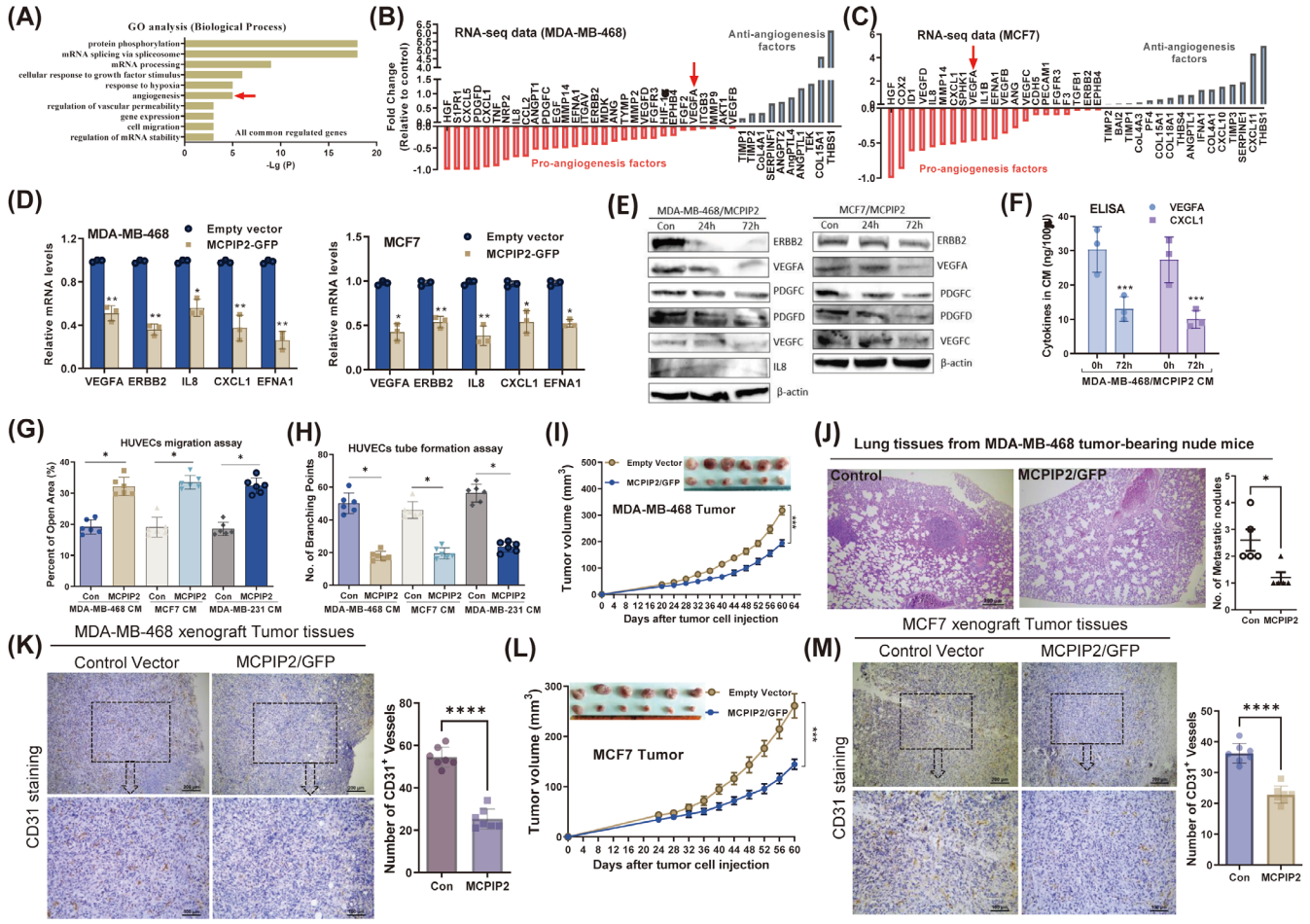

FIGURE 2 | MCPIP2 regulates the expression of angiogenesis-related genes in breast cancer cells and inhibits breast tumor-induced angiogenesis. (A) GO (Gene Ontology) analysis of the regulated genes by MCPIP2 using DAVID (https://david.ncifcrf.gov/), and the 'angiogenesis' term was indicated by red arrow. (B, C) RNA-seq data showing the proangiogenic mRNAs were downregulated, and the antiangiogenic mRNAs were upregulated by MCPIP2 in MDA-MB-468 cells (B) and MCF7 cells (C). (D) qRT-PCR confirming that the expression of indicated proangiogenic genes was downregulated by MCPIP2 in breast tumor cells. (E) Protein expression of the indicated proangiogenic factors was measured by western blotting in MDA-MB-468/MCPIP2 (left) and MCF7/MCPIP2 (right) cells. (F) ELISA quantification of VEGFA and CXCL1 in serum-free culture medium of MDA-MB-468/MCPIP2 cells. (G) Quantification of the percentage of open area of HUVECs treated with indicated tumor CMs in wound-healing assay. (H) Quantification of the number of branching points of HUVECs treated with indicated tumor CMs in tube formation assay. (I) Tumors and the growth curves in nude mice received MDA-MB-468/MCPIP2-GFP and MDA-MB-468/GFP control cells. (J) H&E staining of lung tissue sections from nude mice bearing MDA-MB-468/GFP or MDA-MB-468/MCPIP2-GFP tumors. Scale bar, 100 μm. Quantification of metastatic nodules were shown in the right panel. (K) Representative histological images from MDA-MB-468 xenograft stained with anti-CD31 antibody. Scale bar, 50 μm. Quantification of the number of $CD31^+$ vessels per section (right). (L) Tumors and the growth curves of the MCF7 xenograft model. (M) Representative histological images from MCF7 xenograft stained with anti-CD31 antibody (left) and quantification of the number of $CD31^+$ vessels per section (right). Scale bar, 50 μm. Data are shown as mean ± SD; $^*p < 0.05$, $^{**}p < 0.001$, and $^{****}p < 0.00001$ in unpaired *t*-test.

formation (Figures 2H and S2E). In vivo experiments revealed that MCPIP2 overexpression suppressed MDA-MB-468 breast tumor growth (Figure 2I) and lung metastasis (Figure 2J) in nude mice compared with those in control mice. Notably, the number of CD31-positive vessels in MCPIP2-overexpressing tumors was significantly reduced in MDA-MB-468 xenograft tumors (Figure 2K). The strong suppression of tumor growth (Figure 2L), lung metastases (Figure S2F), and angiogenesis (Figure 2M) by MCPIP2 was also observed in the MCF7 breast tumor model. These results confirmed that MCPIP2 could inhibit breast tumor-induced angiogenesis by modulating angiogenesis-related gene expression.

3.3 | MCPIP2 Inhibits Breast Tumor Angiogenesis by Specifically Destabilizing Proangiogenic mRNAs via the RNase Domain

As an RBP, we next identified the genes in the angiogenesis pathway bound by MCPIP2 using RNA immunoprecipitation (RIP) followed by real-time PCR. Proangiogenic genes (*VEGFA*, *ERBB2*, *IL8*, *EFNA1*, and *CXCL1*), but not antiangiogenic genes (*COL15A1*, *TIMP1*, *SERPINF1*, *ANGPTL1*, and *CXCL11*), were significantly enriched in the MCPIP2 binding complex pulled down with anti-MCPIP2 antibody from cytoplasmic extracts (Figure 3A). We further confirmed

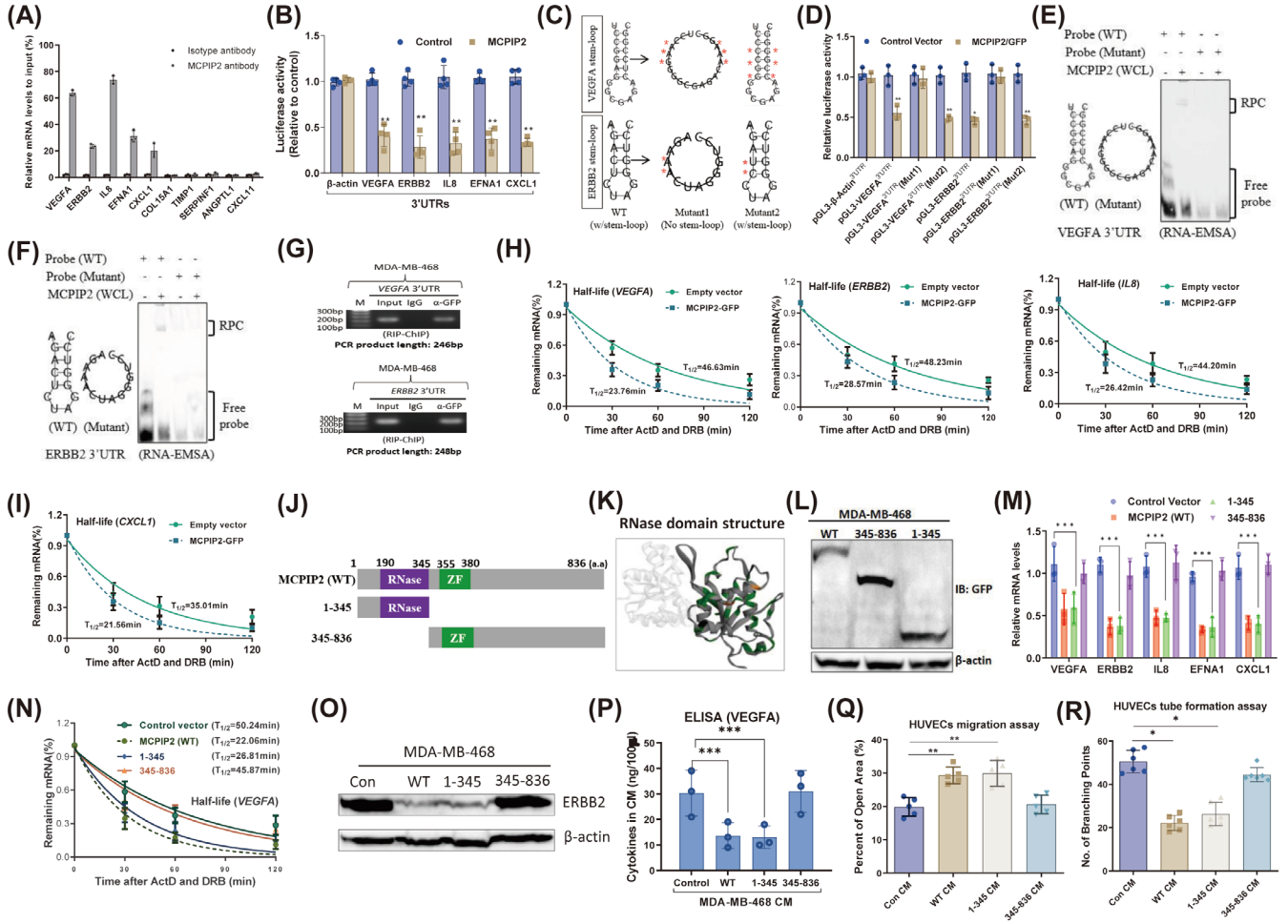

FIGURE 3 | MCPIP2 specifically destabilizes proangiogenic mRNAs and inhibits tumor angiogenesis via the RNase domain. (A) RNA-IP followed by qRT-PCR detection showing that proangiogenic genes but not antiangiogenic genes were enriched by MCPIP2. (B) Measurement of luciferase activities of reporters containing the 3′UTRs of indicated proangiogenic genes. (C) The predicted stem–loop structures of *VEGFA* (top) and *ERBB2* (bottom) in their 3′UTRs and mutation strategy (red asterisks indicate base substitution). Mutant1 becomes unable to form stem–loop structure (middle) and Mutant2 still forms a stem–loop structure (left). (D) Luciferase activity of HEK293 cells transfected with indicated reporters and MCPIP2 expression plasmids. (E, F) RNA-EMSA detection of the RNA-protein complex (RPC) formed using biotin-labeled *VEGFA* (E) or *ERBB2* (F) RNA stem–loop probes and whole-cell lysates (WCL) extracted from MDA-MB-468/MCPIP2-GFP cells. (G) The in vivo binding of MCPIP2 and stem–loop sequences was examined by RIP-ChIP with genome fragments from MDA-MB-468/MCPIP2-GFP cells. The pulled down stem–loop sequences of *VEGFA* (upper) and *ERBB2* (down) were amplified by PCR with primers flanking the stem–loop structures, respectively. (H, I) Half-lives of indicated proangiogenic mRNAs were shortened by MCPIP2 in MDA-MB-468 cells. (J) Schematic representation of the domains in MCPIP2 and the truncated mutants. (K) 3D structure of RNase domain was displayed with the cBioPortal tool (cBioPortal for Cancer Genomics). (L) Expression of MCPIP2 truncations was confirmed by immunoblotting with anti-GFP antibody. (M) Expression of indicated proangiogenic mRNAs was measured by qRT-PCR in MDA-MB-468 cells overexpressing MCPIP2 or its mutants. (N) Half-lives of VEGFA mRNA were measured after overexpressed MCPIP2 or its mutants in MDA-MB-468 cells. (O) ERBB2 and β-actin protein expression were analyzed by western blotting in MDA-MB-468 cells overexpressing MCPIP2 or its mutants. (P) ELISA quantification of VEGFA in serum-free culture medium of MDA-MB-468 cells overexpressing MCPIP2 or its mutants. (Q) Quantification of open area of HUVECs treated with indicated tumor CMs in the wound-healing assay. (R) Quantification of the number of branching points of HUVECs treated with indicated tumor CMs in the tube formation assay. Data are presented as mean ± SD; *$p < 0.05$, **$p < 0.001$, ***$p < 0.0001$ in unpaired *t*-test.

that MCPIP2 could suppress the luciferase activity of reporters containing different proangiogenic factor gene 3′UTRs (Figures 3B and S3A) but had no effect on reporters containing different antiangiogenic gene 3′UTRs (Figure S3B,C), suggesting that MCPIP2 specifically targets the 3′UTRs of proangiogenic mRNAs. Previous research has shown that MCPIP1/2 binds to the structured RNA motif in the 3′UTR of mRNAs [27]. We aligned the 3′UTR sequences of five proangiogenic transcripts among different species and identified a conserved sequence that could form a structural stem–loop conformation (Figure S3D–H). To confirm whether the stem–loop structure is necessary for the MCPIP2-mediated degradation of proangiogenic mRNAs, two different 3′UTR mutant reporters of *ERBB2* and *VEGFA* were generated. The stem–loop structure of mutant1 was deleted by replacing two or six nucleotides, and the stem–loop structure of mutant 2

remained despite the substitution of nucleotides (Figure 3C). Mut1 completely inhibited MCPIP2, while mut2 was still sensitive to MCPIP2 suppression (Figure 3D). RNA-EMSA revealed that a unique RNA–protein complex formed only with the WT probe but not with the mutant probes (Figure 3E,F), suggesting the physical interaction between MCPIP2 and the RNA stem–loop structures of *VEGFA* and *ERBB2*. Furthermore, the RNA immunoprecipitation-chromatin immunoprecipitation (RIP-ChIP) results confirmed that the stem–loop sequences in the 3′UTRs of *VEGFA* and *ERBB2*could be amplified in the anti-GFP antibody pulldown group but not in the isotype IgG group (Figure 3G), indicating that MCPIP2 could bind to the 3′UTRs of proangiogenic mRNAs in vivo.

Because MCPIP family proteins can degrade mRNAs [28], we tested whether MCPIP2 affects the mRNA stability of proangiogenic mRNAs. The half-lives of proangiogenic mRNAs, including *VEGFA*, *ERBB2*, *IL8*, *EFNA1*, and *CXCL1*, were shortened by approximately 1-fold in MCPIP2-overexpressing tumor cells (Figure 3H,I). However, overexpression of MCPIP2 had little effect on the half-lives of antiangiogenic mRNAs (Figure S4A), indicating that MCPIP2 preferentially destabilizes proangiogenic mRNAs rather than antiangiogenic mRNAs.

To identify the domain of MCPIP2 required for the destabilization of proangiogenic mRNAs, two truncated mutants of MCPIP2 were generated: amino acids (aa) 1–345 (containing the conserved RNase domain) and aa 345–836 (containing zinc finger domain) (Figure 3J). The 3D structure of the RNase domain is shown in Figure 3K. The expression of the truncations was confirmed by western blot (Figure 3L). Wild-type (wt) and mutant aa 1–345 could effectively inhibit the mRNA expression (Figure 3M) and half-lives (Figures 3N and S4B) of proangiogenic genes, whereas the aa 345–836 mutant completely lost its inhibitory effects. We also demonstrated that MCPIP2 (WT) and mutant aa 1–345 could downregulate the protein expression of ERBB2 (Figure 3O) and VEGFA (Figure 3P) but that aa 345–836 had no effect. Moreover, CMs from MDA-MB-468 cells expressing WT or the aa 1–345 mutant inhibited HUVEC migration (Figures 3Q and S4C) and tube formation (Figures 3R and S4D). These results demonstrated that MCPIP2 could downregulate the expression of proangiogenic genes by destabilizing their mRNAs, and its RNase domain was required for the inhibition of tumor angiogenesis.

3.4 | RPS3A Interacts With MCPIP2 and Impairs the Degradation of Proangiogenic mRNAs in Breast Tumor Cells

Next, we explored MCPIP2-associated proteins via protein immunoprecipitation (protein IP) combined with mass spectrometry. Several unique bands were observed in the immunoprecipitates from MCPIP2-GFP fusion protein-expressing MDA-MB-468 cells compared with those from GFP-expressing control cells (Figure 4A). The 20 proteins most likely to interact with MCPIP2 according to their molecular weight, coverage percentage, and peptide number are listed (Figure 4B). Many ribosomal proteins, such as ribosomal protein s3a (RPS3A), ribosomal protein s6 (RPS6), ribosomal protein L7A (RPL7A), and ribosomal protein s4, X isoform (RPS4X), have been identified (Table S2). RPS3A was selected for further study because of its relatively high coverage percentage and peptide number. Indeed, MCPIP2-GFP coprecipitated RPS3A, but the GFP control was confirmed via protein IP followed by western blot analysis (Figure 4C). We further demonstrated that MCPIP2 and RPS3A were colocalized in the cytoplasm of breast tumor cells (Figure 4D). These results suggested that MCPIP2 physically interacts with RPS3A. Notably, other proteins identified by mass spectrometry might also interact with MCPIP2, so we analyzed the protein–protein interaction (PPI) network between these proteins using STRING (https://string-db.org/). A PPI network consisting of four modules was constructed from the pulled-down proteins (Figure 4E). Interestingly, GO analysis indicated that these four modules were principally involved in ribosome biogenesis, RNA metabolic processes, and regulation of mRNA stability. These computational analyses further suggested that proteins that interact with MCPIP2 might affect its ability to destabilize mRNA. Indeed, RPS3A was knocked down by shRNAs in MDA-MB-468 cells (Figure 4F), which attenuated the ability of MCPIP2 to reduce the expression (Figure 4G) and mRNA stability (Figure 4H) of *VEGFA* and *ERBB2*. We also found that the expression level of RPS3A was significantly associated with the survival of breast cancer patients (Figure 4I). Overall, these findings indicated that RPS3A was able to interact with MCPIP2 and affect its ability to degrade proangiogenic mRNAs in breast tumor cells.

3.5 | MCPIP2 Depletion Increased Proangiogenic mRNAs Stability and Promoted Tumor Angiogenesis

To further confirm the inhibitory effects of MCPIP2 on breast tumor-induced angiogenesis, we knocked down MCPIP2 in breast tumor cells using two different shRNAs. Approximately, 64% and 59% of MCPIP2 protein expression was silenced by shRNA#1 and shRNA#2, respectively (Figure 5A). Knockdown of MCPIP2 significantly increased the mRNA expression of the proangiogenic genes in breast tumor cells (Figure 5B). Moreover, the expression of these proangiogenic genes was also increased in MCPIP1$^{-/-}$ CD4 + T cells (Figure S5A) and mouse embryonic fibroblasts (MEFs) (Figure S5B) [27]. In contrast, no change in the mRNA expression of antiangiogenic genes was detected after MCPIP2 knockdown (Figure S5C). Consistent with the overexpression results, MCPIP2 knockdown prolonged the half-lives of proangiogenic mRNAs in breast tumor cells (Figures 5C–E and S5D). The VEGFA, CXCL1, and ERBB2 protein levels were increased upon MCPIP2 knockdown in breast tumor cells (Figure 5F,G). CMs from MDA-MB-468/shMCPIP2 cells significantly promoted HUVEC migration (Figures 5H and S5E) and tube formation (Figures 5I and S5F). To further confirm that proangiogenic genes are involved in MCPIP2-mediated inhibition of tumor angiogenesis, the *VEGFA* and *CXCL1* genes were knocked down by shRNA lentiviruses in MDA-MB-468/shMCPIP2 cells (Figure 5J). HUVEC migration was partially restored to a level comparable to that in the control group after co-knockdown of *MCPIP2* and its targets *VEGFA* and *CXCL1* (Figures 5K and S5G), suggesting that proangiogenic genes

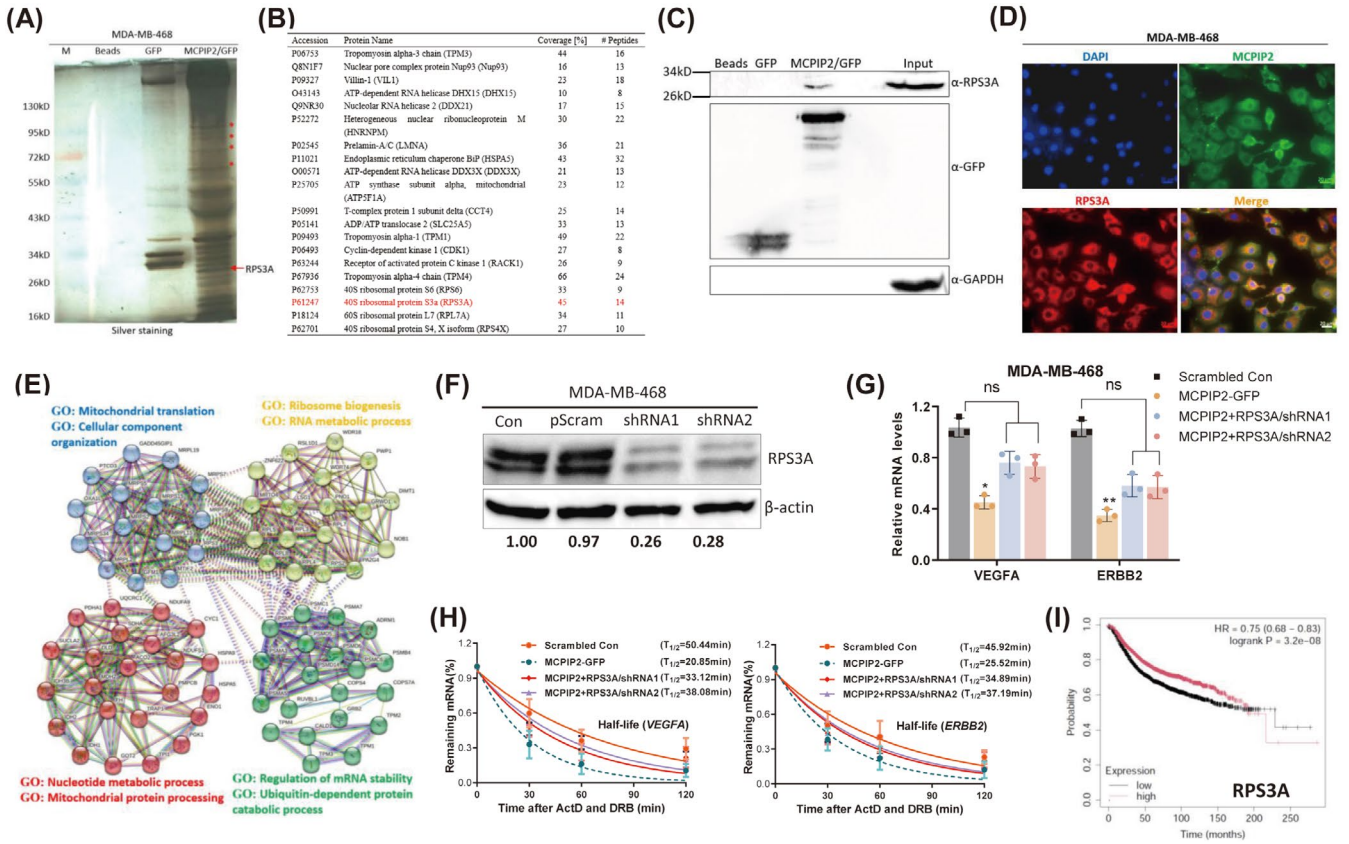

FIGURE 4 | RPS3A interacts with MCPIP2 and impairs its proangiogenic mRNA degradation in breast tumor cells. (A) Silver staining of gel separating MCPIP2-associated proteins. (B) Top 20 MCPIP2-associated proteins identified by MS. (C) MCPIP2 coprecipitated with RPS3A in MDA-MB-468 cells was confirmed by pull-down assay followed by immunoblotting. (D) The colocalization of MCPIP2 and RPS3A in breast tumor cells was observed by immunocytochemistry. (E) The protein–protein interaction network of MCPIP2-associated proteins was analyzed by the STRING tool (https://string-db.org/). (F) Immunoblotting confirmed the knockdown of RPS3A protein expression in MDA-MB-468 cells. (G) *VEGFA* and *ERBB2* mRNA expression was measured by qRT-PCR. (H) MCPIP2-mediated mRNA degradation of *VEGFA* and *ERBB2* was measured in RPS3A knockdown cells. (I) Relapse-free survival curves of breast cancer patients with low and high RPS3A transcripts. Data are presented as mean ± SD; $^{*}p < 0.05$ and $^{**}p < 0.001$ in unpaired *t*-test. ns, non significance.

are indeed involved in the MCPIP2-mediated inhibition of tumor angiogenesis.

3.6 | IGF2BP1 Interacts With the Common Stem–Loop Structure of VEGFA While Stabilizing Its mRNA and Promoting Proangiogenic Gene Expression and Breast Tumor Angiogenesis

Given that VEGFA is highly expressed in breast cancer, and our results showed that MCPIP2 downregulated VEGFA expression by destabilizing its mRNA via binding to the stem–loop structure, it is reasonable to speculate that other proteins should exist to stabilize *VEGFA* mRNA in breast tumor cells. A conserved *VEGFA* 3′UTR sequence can be folded into a stem–loop structure among different species, which indicates that the stem–loop structure might be important for VEGFA gene expression in mammals (Figure 6A). To identify the proteins that bind to the stem–loop structure of *VEGFA* inside breast tumor cells, RNA pull-down was performed with a biotin-labeled RNA stem–loop probe and a linearized RNA probe (the stem–loop structure was removed by heating RNA probe to 95°C and then rapidly quenched to 4°C). Several unique bands were observed in the immunoprecipitates from the stem–loop probe (w/SL) compared with those from the linearized probe (NO SL) controls (Figure 6B). The top 15 proteins associated with the stem–loop structure were listed according to their molecular weight, coverage percentage, and peptide number (Figure 6C and Table S3). Notably, many of the proteins pulled down were RNA-binding proteins, such as IGF2BP1/3 [29], DEAD-box RNA helicase (DDX5) [30] and polypyrimidine tract-binding protein 1 (PTBP1) [31], which further verified our RNA pull-down assay. Interestingly, studies have shown that some of these RBPs also target RNA secondary structures [30, 32]. IGF2BP1 was selected for further study because of its high coverage percentage and peptide number. Indeed, the results from RNA pull-down followed by western blot detection (Figure 6D), RNA-EMSA (Figure 6E), and RIP-ChIP (Figure 6F) confirmed the interaction between IGF2BP1 and the stem–loop of *VEGFA* in breast tumor cells.

Next, our RNA sequencing data showed that IGF2BP1 overexpression (Figure S6A) increased the expression of proangiogenic genes (Figures 6G and S6B) and decreased the expression of antiangiogenic genes (Figure S6C,D and Table S4) in breast tumor cells. IGF2BP1 was able to enhance the mRNA expression

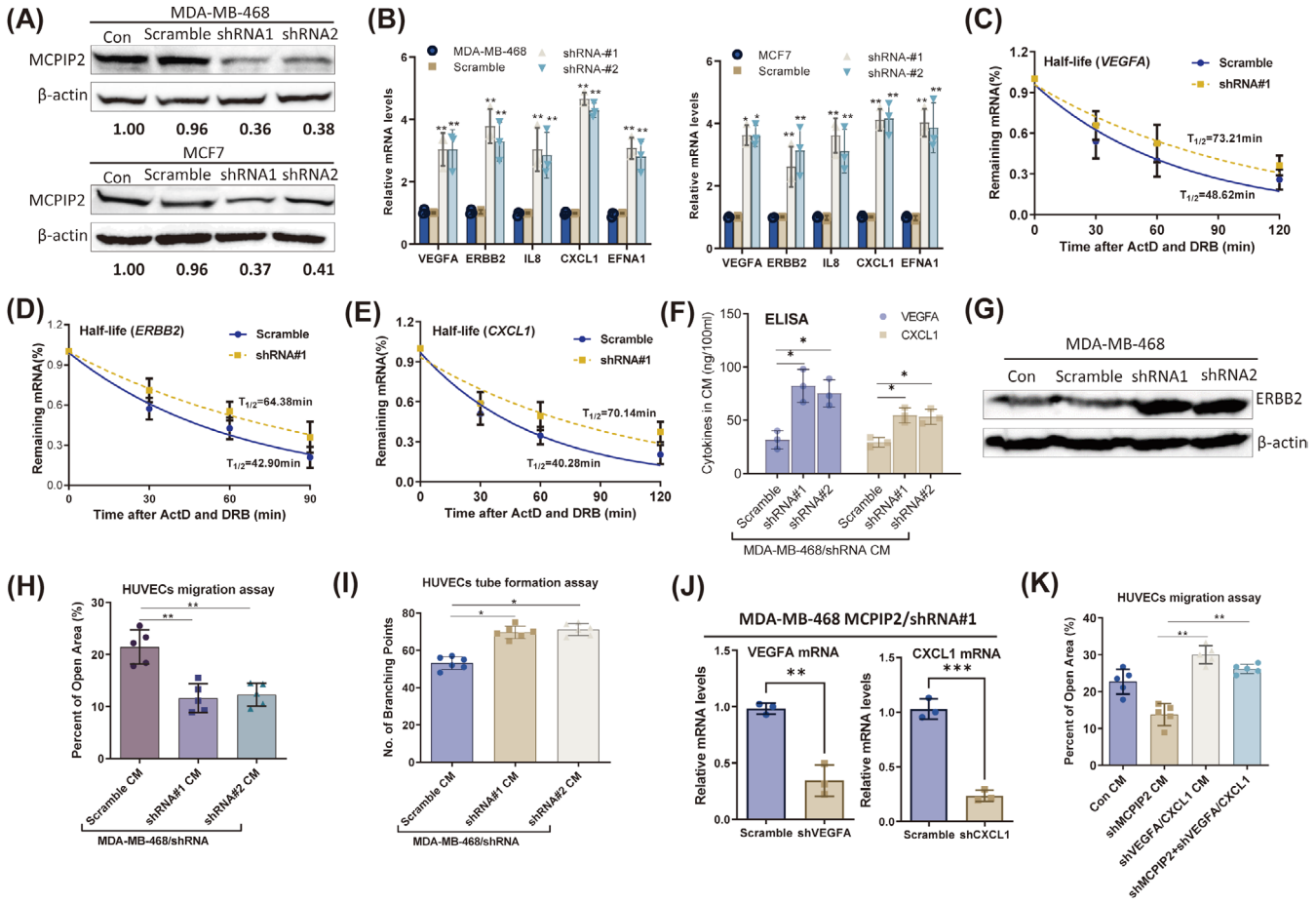

FIGURE 5 | MCPIP2 depletion increased proangiogenic mRNAs stability and promoted tumor angiogenesis. (A) MCPIP2 protein expression was knockdown by infecting MCPIP2-shRNAs/lentivirus and scramble-control/lentivirus in MDA-MB-468 and MCF7 cells, respectively. Western blot quantification was assessed by ImageJ. (B) Expression of proangiogenic mRNAs was measured by qRT-PCR in MDA-MB-468 (left) and MCF7 (right) cells, respectively, after knocking down MCPIP2. (C–E) Half-lives of indicated proangiogenic mRNAs were increased after MCPIP2 knockdown in MDA-MB-468 cells. (F) ELISA quantification of VEGFA and CXCL1 in serum-free culture medium of MCPIP2-knocking down MDA-MB-468 cells. (G) ERBB2 and β-actin protein expression were measured by western blotting in MCPIP2 knocked down MDA-MB-468 cells. (H) Quantification of open area of HUVECs treated with indicated tumor CMs in the wound-healing assay. (I) Quantification of the number of branching points of HUVECs treated with indicated tumor CMs. (J) MDA-MB-468/shMCPIP2 cells were infected with scramble/lentivirus or shRNA-lentivirus targeting *VEGFA* and *CXCL1*, respectively. Total RNA extracted to measure mRNAs of *VEGFA* and *CXCL1*. (K) Quantification of open area of HUVECs treated with indicated tumor CMs. Data are presented as mean ± SD; $^{*}p < 0.05$, $^{**}p < 0.001$, and $^{***}p < 0.0001$ in unpaired *t*-test.

(Figure 6H) and half-lives of *VEGFA*, *ERBB2*, *IL8*, *CXCL1*, and *EFNA1* in breast tumor cells (Figure S6E). Western blot results also showed that IGF2BP1 can promote the expression of proangiogenic factors (Figure S6F). Interestingly, although the proangiogenic genes regulated by MCPIP2 and IGF2BP1 are not completely matched, the two RBPs regulated these genes in a clear opposite trend (Figures 2B, 6G and S6B). GO analysis also suggested that the regulated genes by IGF2BP1 were also strongly enriched for transcripts associated with angiogenesis (Figure 6I). We further found that IGF2BP1 can attenuate MCPIP2-facilitated *VEGFA* mRNA suppression (Figure 6J) and destabilization (Figure 6K).

In contrast to the lower expression of MCPIP2 in human breast cancer (Figure 1), the expression of *IGF2BP1* in breast tumors was increased (Figure S6G–I). Survival analysis also revealed that breast cancer patients with lower *IGF2BP1* levels tended to survive (Figure S6J), which is opposite to the survival curve of patients with lower MCPIP2 levels (Figure 1K). It is not surprising that IGF2BP1 overexpression promoted breast tumor growth (Figure 6L), which is consistent with previous reports [33, 34]. Notably, there were significantly more CD31+ microvessels in the IGF2BP1-overexpressing xenograft group than in the control group (Figure 6M). Overall, our findings indicated that IGF2BP1 can increase the mRNA stability of proangiogenic genes by targeting the stem–loop structure in the 3′UTR and promoting breast tumor angiogenesis.

3.7 | IGF2BP1 and MCPIP2 Potentially Antagonize Breast Tumor Angiogenesis

To avoid the effects of gene manipulation, we simulate the clinical treatment of breast cancer by administering adenovirus expressing MCPIP2/GFP fusion gene and the control virus (expressing GFP) in the established MDA-MB-468 breast tumors in nude mice. Upon tumor mass reaching a diameter of ~5 mm, 10^{10} pfu/100 uL PBS adenovirus was injected every other day for

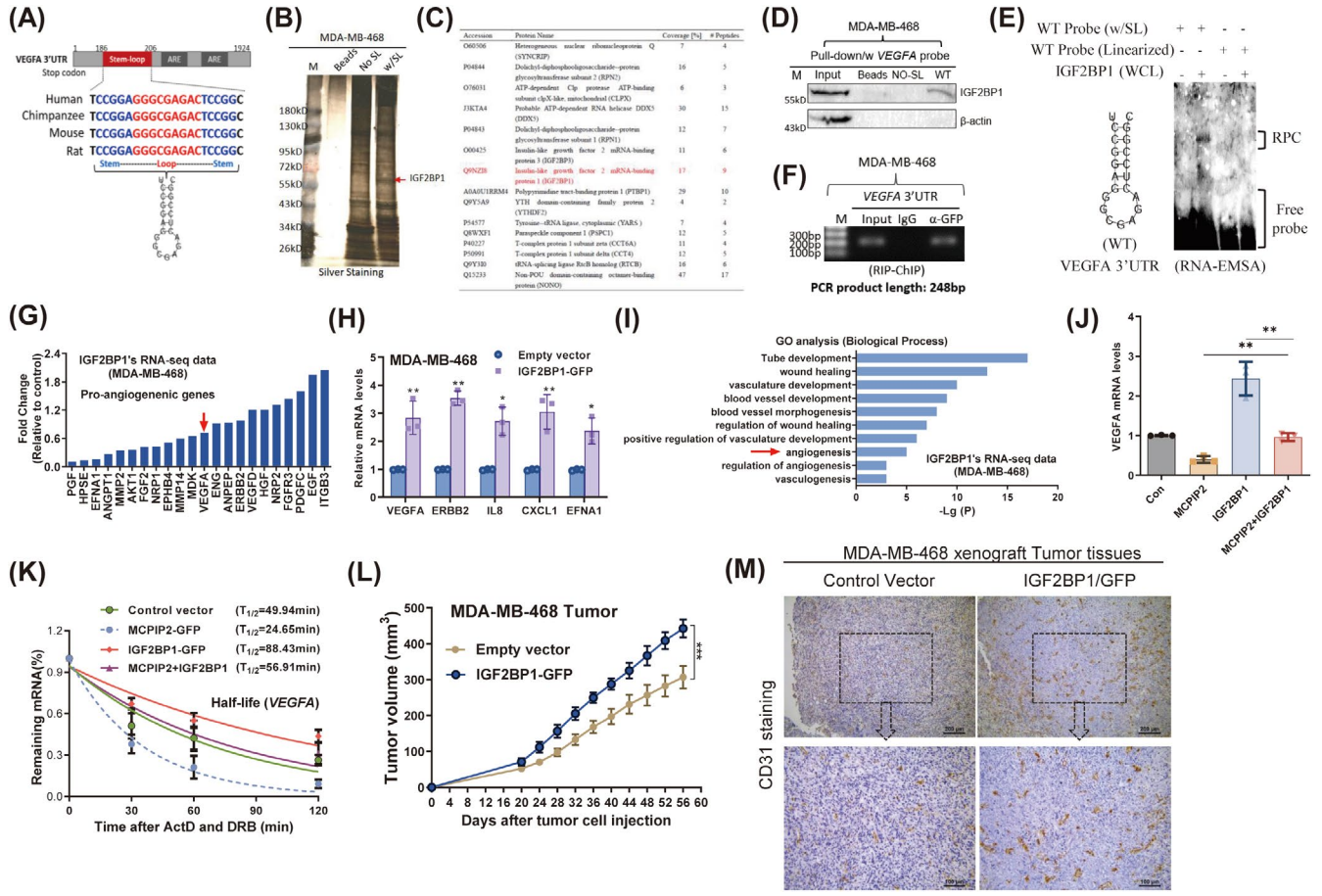

FIGURE 6 | IGF2BP1 interacts with the common stem–loop structure of *VEGFA* while stabilize its mRNA and enhances proangiogenic genes expression. (A) Schematic representation of the stem–loop structure in human *VEGFA* 3′UTR and alignment of conserved stem–loop sequences in different species. (B) Silver staining of proteins pulled down by the human *VEGFA* RNA stem–loop structure in MDA-MB-468 cells. (C) The top 15 proteins associated with *VEGFA* stem–loop structure were listed. (D) Immunoblotting analysis of IGF2BP1 coprecipitated with the *VEGFA* stem–loop probe in MDA-MB-468 cells. (E) RNA-EMSA detection of the RNA-protein complex (RPC) formed using indicated biotin-labeled RNA probes and whole-cell lysates (WCL) extracted from MDA-MB-468/IGF2BP1-GFP cells. (F) RIP-ChIP analysis of IGF2BP1 bound to the *VEGFA* stem–loop sequence in MDA-MB-468/IGF2BP1-GFP cells. (G) RNA sequencing data showed that the proangiogenic mRNAs were upregulated by IGF2BP1 in MDA-MB-468 cells. (H) qRT-PCR analysis of the expression of indicated proangiogenic genes in IGF2BP1-overexpressing MDA-MB-468 cells. (I) GO analysis of the regulated genes by IGF2BP1 in MDA-MB-468 cells, and the 'angiogenesis' term was indicated by arrow. (J) qRT-PCR was performed to verify the regulatory effects of MCPIP2 and IGF2BP1 on *VEGFA* in MDA-MB-468 cells. (K) Half-lives analysis of *VEGFA* affected by MCPIP2 and IGF2BP1 in MDA-MB-468 cells. (L) Tumor volume of implantation tumors. (M) Representative histological images from GFP-expressing (control vector) or IGF2BP1/GFP-expressing MDA-MB-468 xenografts stained with the anti-CD31 antibody. Scale bar, 50 μm. Data are represented as mean ± SD. *$p < 0.05$, **$p < 0.01$ in unpaired *t*-test.

five times (Figure 7A). The growth rate of tumors treated with MCPIP2-expressing adenovirus was clearly slower than that of those treated with control adenovirus (Figure 7B). At the end of the experiment, the size of the tumor injected with MCPIP2-expressing adenovirus was significantly diminished compared with that of the control group (Figure 7B). Additionally, treatment with MCPIP2-expressing adenovirus significantly reduced the number of metastatic foci in the lung tissue (Figure 7C). These results highlight the therapeutic potential of MCPIP2 on breast cancer progression in vivo. We further found that *VEGFA* and *ERBB2* expression was significantly decreased in MCPIP2-expressing xenografts (Figure 7D), whereas it increased in IGF2BP1-expressing xenografts (Figure 7E). Moreover, a significant negative correlation was observed between *MCPIP2* expression and *VEGFA*, *ERBB2*, *EFNA1*, *IL8*, and *CXCL1* expression in human breast cancer samples (Figures 7F and S7A). However, there was a significant positive correlation between *IGF2BP1* expression and the expression of the above proangiogenic genes (Figures 7G and S7B). Importantly, more CD31-positive microvessels were observed in MCPIP2-negative breast tumors than in MCPIP2-positive tumors (Figure 7H). However, there were significantly more CD31-positive microvessels in IGF2BP1-positive breast tumors (Figure 7I). These findings further suggested that MCPIP2 and IGF2BP1 might antagonize the regulation of breast tumor angiogenesis.

Finally, we proposed a model to elucidate the potential roles of MCPIP2 and IGF2BP1 in regulating breast tumor angiogenesis. MCPIP2 decays proangiogenic mRNAs by binding to the conserved stem–loop structure in the 3′ UTR of these transcripts via its RNase domain, resulting in inhibition of proangiogenic gene expression and breast tumor angiogenesis. In contrast,

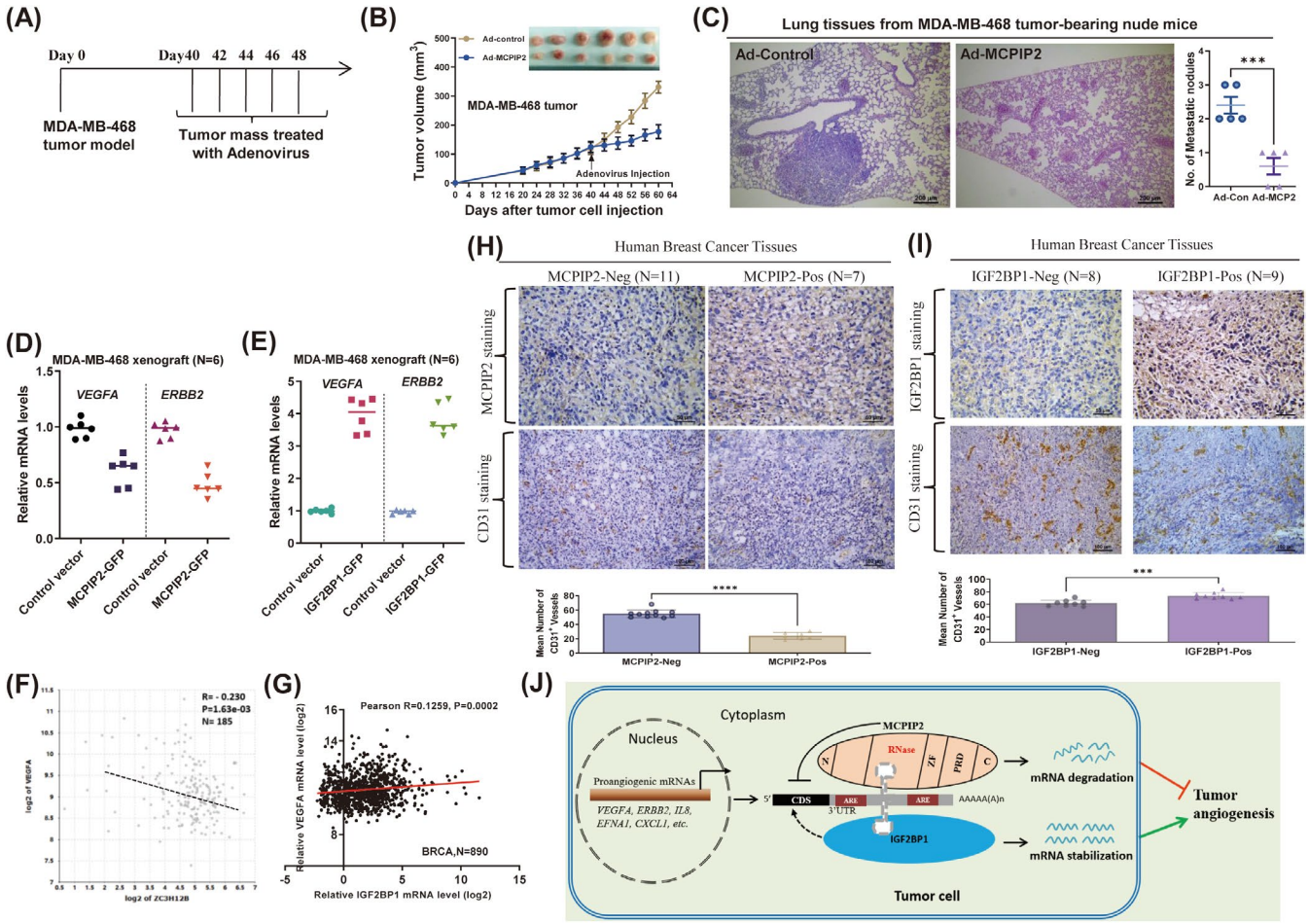

FIGURE 7 | IGF2BP1 and MCPIP2 potentially antagonize proangiogenic genes expression and breast tumor angiogenesis. (A) A flow chart of adenovirus administration for tumor treatment. (B) The growth curves of MDA-MB-468 tumors treated with adenovirus. (C) H&E staining of lung tissue sections from nude mice bearing MDA-MB-468 tumors treated with MCPIP2-expressing adenovirus or control adenovirus, respectively. Scale bar, 200 μm. Quantification of metastatic nodules is shown in the right panel. (D and E) The mRNA expression levels of *VEGFA* and *ERBB2* were measured by qRT-PCR in MCPIP2-overexpressing (D) and IGF2BP1-overexpressing (E) xenografts and their control groups, respectively. (F and G) Pearson's correlation analysis between *MCPIP2* (F), *IGF2BP1*, (G) and *VEGFA* expression in human breast cancer patients were performed with R2 (http://r2.amc.nl) (F) and OncoLnc (http://www.oncolnc.org/) (G) online tools. (H, I) Representative images of IHC staining for MCPIP2 (H, upper), IGF2BP1 (I, upper), and CD31 (lower) in human breast cancer tissues. Scale bars, 50 or 100 μm. (J) A proposed model showed that the pro-angiogenic transcripts can be destabilized by MCPIP2 or stabilized by IGF2BP1 in breast tumor cells. Data are shown as mean ± SD; ***$p < 0.0001$, ****$p < 0.00001$ in unpaired *t*-test.

IGF2BP1 stabilized proangiogenic mRNAs by binding to the common stem–loop structure, leading to the promotion of pro-angiogenic gene expression and tumor angiogenesis (Figure 7J). Collectively, these results strongly demonstrated that MCPIP2 and IGF2BP1 may be a pair of potential competitors involved in regulating breast tumor angiogenesis and that inducing MCPIP2 expression while reducing IGF2BP1 in breast tumors might be a promising antiangiogenic therapy for breast cancer.

4 | Discussion

RNA-binding proteins can modulate tumor progression by regulating different signaling pathways and key tumor-associated genes to act as an oncogene or a tumor suppressor [35, 36]. Many RBPs are abnormally expressed in human breast cancer [37]. However, to our knowledge, the expression patterns of RBPs in breast cancer have not been reported. In this study, we demonstrated for the first time the expression of all known RBPs in human breast cancer and revealed an antagonistic role of RBPs in regulating the angiogenesis signaling pathway in breast cancer. Our study demonstrated that MCPIP2 and IGF2BP1, two RBPs, are negatively and positively involved in regulating proangiogenic gene expression and breast tumor-induced angiogenesis, respectively.

To date, the signaling pathways and target genes regulated by MCPIP2 in breast tumor cells have not yet been reported. Initially, we found that MCPIP1 (a homolog of MCPIP2) can inhibit the expression of inflammatory genes that are also related to angiogenesis, such as *cyclooxygenase 2* (*COX2*), *interleukin-6* (*IL6*), and *inhibitor of DNA binding-1* (*ID1*) [27]. Thus, we speculated that MCPIP2 targets angiogenesis-related genes and suppresses tumor-induced angiogenesis in breast cancer. As expected, our RNA sequencing results confirmed that MCPIP2 can regulate the expression of angiogenesis-related genes in

breast tumor cells. Experiments also showed that MCPIP2 was able to inhibit breast tumor-induced angiogenesis both in vitro and in vivo. To our knowledge, there is no direct evidence in the inhibition of tumor angiogenesis by MCPIP2 in breast cancer. MCPIP2-mediated inhibition of breast tumor angiogenesis might be a mechanism against further growth of breast tumors and progression of lung metastasis.

Five proangiogenic genes, *VEGFA*, *ERBB2*, *IL8*, *EFNA1*, and *CXCL1*, were selected as targets of MCPIP2 for further study in breast tumor cells for three reasons: (i) they are regulated by MCPIP2 in two breast tumor cells, (ii) the fold changes in the expression of these genes balance the increases and decreases in expression, and (iii) they are known to be typical proangiogenic genes. Considering our RNA sequencing data, we speculated that the inhibition of breast tumor angiogenesis by MCPIP2 might involve multiple molecular events, as many other proangiogenic genes are also targeted by MCPIP2 rather than these five genes. We found that MCPIP2, as RBP, preferentially binds to proangiogenic mRNAs but not antiangiogenic genes; unfortunately, the underlying mechanism is still unclear. We speculated that this RNA binding selectivity of MCPIP2 may have developed during the long-term evolution of mammals. MCPIP proteins are known to degrade their target mRNAs by themselves through the RNase domain [38]. It has been reported that MCPIP2 also possesses an RNase domain at its N-terminal with endonuclease activity [13, 15]. Here, we demonstrated that the RNase domain is crucial for tumor angiogenesis inhibition by mutating the RNase and zinc finger (ZF) domains. These findings broaden the understanding of the substrates and pathways regulated by MCPIP family proteins.

So far, reports on MCPIP-associated proteins, especially in breast tumor cells, are limited. One previous study showed that MCPIP1 can interact with ribosomal proteins and up frameshift 1 (UPF1) in HeLa cells [27]. Here, for the first time, we identified proteins associated with MCPIP2 in breast tumor cells by protein pull-down combined with mass spectrometry. Like for MCPIP1, many proteins associated with MCPIP2 are ribosomal proteins, such as RPS3A, RPS6, and RPS4X. These findings suggested that MCPIP proteins might be mainly associated with ribosomes for mediating mRNA decay in tumor cells. An open question is how ribosomal proteins affect the RNase activity of MCPIP2; therefore, it will be necessary to further investigate the underlying mechanisms of MCPIP2 in different contexts.

Similar to MCPIP1 [39, 40], MCPIP2 also recognizes and binds to stem–loop structures localized in the 3′UTRs of proangiogenic mRNAs. The secondary conformation of RNA is believed to be a key element for RBP binding and gene expression regulation [24, 41, 42]. Here, we confirmed that the RBP IGF2BP1 was also able to bind to the RNA stem–loop structure of *VEGFA* and stabilize its mRNA. Our findings established an axis linking the RBPs MCPIP2 and IGF2BP1 to the expression of proangiogenic genes. IGF2BP1 is highly expressed in breast cancer and can enhance cancer-associated gene expression by stabilizing mRNAs [43], which further supports our findings. Interestingly, IGF2BP1 was found to promote breast tumor angiogenesis, while MCPIP2 inhibited angiogenesis, which led us to consider that IGF2BP1 might compete with MCPIP2 to regulate breast tumor angiogenesis.

In conclusion, our results demonstrate that MCPIP2 and IGF2BP1 antagonize breast tumor angiogenesis by competitively regulating the mRNA stability and expression of proangiogenic genes via targeting the common RNA stem–loop structure. These findings expand the understanding of the RBP-mediated post-transcriptional regulation of angiogenesis-related genes and highlight the potential of MCPIP2 and IGF2BP1 as a pair of promising targets for antiangiogenic therapy of breast cancer.

Author Contributions

Wenbao Lu designed the study, performed the experiments, analyzed the data, and wrote the manuscript. Hongwei Li, Xueting Liu, and Ailing Li conducted the animal experiments and part of the histological experiments. Ruijuan Xiu reviewed the manuscript. All the coauthors have read and approved the final manuscript for publication.

Acknowledgments

The authors have nothing to report.

Ethics Statement

The study was approved by the Medical Ethics Committee of the Institute of Microcirculation, Chinese Academy of Medical Sciences (CAMS), and Peking Union Medical College (PUMC) in accordance with the Declaration of Helsinki. All animal experimental procedures have been approved by the Experimental Animal Care and Ethics Committee of the Institute of Microcirculation, CAMS, and PUMC.

Consent

All subjects gave their informed consent for inclusion before they participated in the study.

Conflicts of Interest

The authors declare no conflicts of interest.

Data Availability Statement

All data supporting the findings of this study are included in the article and/or the Supporting Information. The RNA sequencing data from this study are deposited in the Sequence Read Archive (SRA) database under projects PRJNA1119197 and PRJNA1119237. The MS data are available via ProteomeXchange with the IDs: PXD052919 and PXD052920.

References

1. R. Lugano, M. Ramachandran, and A. Dimberg, "Tumor Angiogenesis: Causes, Consequences, Challenges and Opportunities," *Cellular and Molecular Life Sciences* 77 (2020): 1745–1770.

2. E. Iivanainen and K. Elenius, "ErbB Targeted Drugs and Angiogenesis," *Current Vascular Pharmacology* 8 (2010): 421–431.

3. Y. Kang, H. Li, Y. Liu, and Z. Li, "Regulation of VEGF-A Expression and VEGF-A-Targeted Therapy in Malignant Tumors," *Journal of Cancer Research and Clinical Oncology* 150 (2024): 221.

4. K. Matsushima, D. Yang, and J. J. Oppenheim, "Interleukin-8: An Evolving Chemokine," *Cytokine* 153 (2022): 155828.

5. J. Korbecki, K. Barczak, I. Gutowska, D. Chlubek, and I. Baranowska-Bosiacka, "CXCL1: Gene, Promoter, Regulation of Expression, mRNA Stability, Regulation of Activity in the Intercellular Space," *International Journal of Molecular Sciences* 23 (2022): 792.

6. Y. Hao and G. Li, "Role of EFNA1 in Tumorigenesis and Prospects for Cancer Therapy," *Biomedicine & Pharmacotherapy* 130 (2020): 110567.

7. H. Jiang, M. Liu, Y. Qin, and H. Zhang, "miR-9 Promotes Canine Endothelial-Like Cell Migration by Targeting COL15A1," *Veterinary Medicine and Science* 10 (2024): e1339.

8. S. Zacchigna, L. Zentilin, M. Morini, et al., "AAV-Mediated Gene Transfer of Tissue Inhibitor of Metalloproteinases-1 Inhibits Vascular Tumor Growth and Angiogenesis In Vivo," *Cancer Gene Therapy* 11 (2004): 73–80.

9. Y. Wang, X. Liu, X. Quan, et al., "Pigment Epithelium-Derived Factor and Its Role in Microvascular-Related Diseases," *Biochimie* 200 (2022): 153–171.

10. Q. Gao and Y. Zhang, "CXCL11 Signaling in the Tumor Microenvironment," *Advances in Experimental Medicine and Biology* 1302 (2021): 41–50.

11. D. Wang, H. Li, T. Zeng, et al., "Exosome-Transmitted ANGPTL1 Suppresses Angiogenesis in Glioblastoma by Inhibiting the VEGFA/VEGFR2/Akt/eNOS Pathway," *Journal of Neuroimmunology* 387 (2024): 578266.

12. F. H. Al-Ostoot, S. Salah, H. A. Khamees, and S. A. Khanum, "Tumor Angiogenesis: Current Challenges and Therapeutic Opportunities," *Cancer Treatment and Research Communications* 28 (2021): 100422, https://doi.org/10.1016/j.ctarc.2021.100422.

13. T. Mino and O. Takeuchi, "Regnase-1-Related Endoribonucleases in Health and Immunological Diseases," *Immunological Reviews* 304 (2021): 97–110.

14. J. Liang, J. Wang, A. Azfer, et al., "A Novel CCCH-Zinc Finger Protein Family Regulates Proinflammatory Activation of Macrophages," *Journal of Biological Chemistry* 283 (2008): 6337–6346.

15. M. Wawro, K. Wawro, J. Kochan, et al., "ZC3H12B/MCPIP2, a New Active Member of the ZC3H12 Family," *RNA* 25 (2019): 840–856.

16. W. Sowinska, M. Wawro, D. D. Biswas, et al., "The Homeostatic Function of Regnase-2 Restricts Neuroinflammation," *FASEB Journal* 37 (2023): e22798.

17. A. Jolma, J. Zhang, E. Mondragon, et al., "Binding Specificities of Human RNA-Binding Proteins Toward Structured and Linear RNA Sequences," *Genome Research* 30, no. 7 (2020): 962–973, https://doi.org/10.1101/gr.258848.119.

18. Y. S. Ma, T. M. Wu, C. C. Ling, et al., "M2 Macrophage-Derived Exosomal MicroRNA-155-5p Promotes the Immune Escape of Colon Cancer by Downregulating ZC3H12B," *Molecular Therapy—Oncolytics* 20 (2021): 484–498.

19. Y. Huang, M. Xu, C. Jing, X. Wu, X. Chen, and W. Zhang, "Extracellular Vesicle-Derived miR-320a Targets ZC3H12B to Inhibit Tumorigenesis, Invasion, and Angiogenesis in Ovarian Cancer," *Discover Oncology* 12 (2021): 51.

20. W. Sowinska, M. Wawro, J. Kochan, et al., "Regnase-2 Inhibits Glioblastoma Cell Proliferation," *Scientific Reports* 14 (2024): 1574.

21. Z. Chen, H. Wu, H. Yang, Y. Fan, S. Zhao, and M. Zhang, "Identification and Validation of RNA-Binding Protein-Related Gene Signature Revealed Potential Associations With Immunosuppression and Drug Sensitivity in Glioma," *Cancer Medicine* 10 (2021): 7418–7439.

22. G. Sharma, T. M. Tran, I. Bansal, et al., "RNA Binding Protein IGF2BP1 Synergizes With ETV6-RUNX1 to Drive Oncogenic Signaling in B-Cell Acute Lymphoblastic Leukemia," *Journal of Experimental & Clinical Cancer Research* 42 (2023): 231.

23. L. Zhang, Y. Wan, Z. Zhang, et al., "IGF2BP1 Overexpression Stabilizes PEG10 mRNA in an m6A-Dependent Manner and Promotes Endometrial Cancer Progression," *Theranostics* 11 (2021): 1100–1114.

24. W. Lu, M. Zhou, B. Wang, X. Liu, and B. Li, "Roquin1 Inhibits the Proliferation of Breast Cancer Cells by Inducing G1/S Cell Cycle Arrest via Selectively Destabilizing the mRNAs of Cell Cycle-Promoting Genes," *Journal of Experimental & Clinical Cancer Research* 39 (2020): 255.

25. S. Bhargava, V. Patil, K. Mahalingam, and K. Somasundaram, "Elucidation of the Genetic and Epigenetic Landscape Alterations in RNA Binding Proteins in Glioblastoma," *Oncotarget* 8 (2017): 16650–16668.

26. E. Sebestyen, B. Singh, B. Minana, et al., "Large-Scale Analysis of Genome and Transcriptome Alterations in Multiple Tumors Unveils Novel Cancer-Relevant Splicing Networks," *Genome Research* 26 (2016): 732–744.

27. T. Mino, Y. Murakawa, A. Fukao, et al., "Regnase-1 and Roquin Regulate a Common Element in Inflammatory mRNAs by Spatiotemporally Distinct Mechanisms," *Cell* 161 (2015): 1058–1073.

28. T. Uehata and S. Akira, "mRNA Degradation by the Endoribonuclease Regnase-1/ZC3H12a/MCPIP-1," *Biochimica et Biophysica Acta* 1829, no. 6–7 (2013): 708–713, https://doi.org/10.1016/j.bbagrm.2013.03.001.

29. J. Fan, M. Zhuang, W. Fan, and M. Hou, "RNA N6-Methyladenosine Reader IGF2BP3 Promotes Acute Myeloid Leukemia Progression by Controlling Stabilization of EPOR mRNA," *PeerJ* 11 (2023): e15706.

30. A. Kar, K. Fushimi, X. Zhou, et al., "RNA Helicase p68 (DDX5) Regulates Tau Exon 10 Splicing by Modulating a Stem-Loop Structure at the 5′ Splice Site," *Molecular and Cellular Biology* 31 (2011): 1812–1821.

31. X. Wang, C. Liang, S. Wang, et al., "RNA Binding Protein PTBP1 Promotes the Metastasis of Gastric Cancer by Stabilizing PGK1 mRNA," *Cells* 13 (2024): 140.

32. S. M. Korn, C. J. Ulshofer, T. Schneider, and A. Schlundt, "Structures and Target RNA Preferences of the RNA-Binding Protein Family of IGF2BPs: An Overview," *Structure* 29 (2021): 787–803.

33. W. Shi, Y. Tang, J. Lu, Y. Zhuang, and J. Wang, "MIR210HG Promotes Breast Cancer Progression by IGF2BP1 Mediated m6A Modification," *Cell & Bioscience* 12 (2022): 38.

34. J. Shi, Q. Zhang, X. Yin, et al., "Stabilization of IGF2BP1 by USP10 Promotes Breast Cancer Metastasis via CPT1A in an m6A-Dependent Manner," *International Journal of Biological Sciences* 19 (2023): 449–464.

35. H. Qin, H. Ni, Y. Liu, et al., "RNA-Binding Proteins in Tumor Progression," *Journal of Hematology & Oncology* 13 (2020): 90.

36. S. Wang, Z. Sun, Z. Lei, and H. T. Zhang, "RNA-Binding Proteins and Cancer Metastasis," *Seminars in Cancer Biology* 86 (2022): 748–768.

37. S. Wang, H. Sun, G. Chen, et al., "RNA-Binding Proteins in Breast Cancer: Biological Implications and Therapeutic Opportunities," *Critical Reviews in Oncology/Hematology* 195 (2024): 104271.

38. W. Lu, H. Ning, L. Gu, et al., "MCPIP1 Selectively Destabilizes Transcripts Associated With an Antiapoptotic Gene Expression Program in Breast Cancer Cells That Can Elicit Complete Tumor Regression," *Cancer Research* 76 (2016): 1429–1440.

39. T. Uehata, H. Iwasaki, A. Vandenbon, et al., "Malt1-Induced Cleavage of Regnase-1 in CD4(+) Helper T Cells Regulates Immune Activation," *Cell* 153 (2013): 1036–1049.

40. M. Li, W. Cao, H. Liu, et al., "MCPIP1 Down-Regulates IL-2 Expression Through an ARE-Independent Pathway," *PLoS One* 7 (2012): e49841.

41. Y. Wan, K. Qu, Q. C. Zhang, et al., "Landscape and Variation of RNA Secondary Structure Across the Human Transcriptome," *Nature* 505 (2014): 706–709.

42. A. Chelkowska-Pauszek, J. G. Kosinski, K. Marciniak, M. Wysocka, K. Bakowska-Zywicka, and M. Zywicki, "The Role of RNA Secondary Structure in Regulation of Gene Expression in Bacteria," *International Journal of Molecular Sciences* 22 (2021): 7845.

43. S. Li and M. Jiang, "Elevated Insulin-Like Growth Factor 2 mRNA Binding Protein 1 Levels Predict a Poor Prognosis in Patients With Breast Carcinoma Using an Integrated Multi-Omics Data Analysis," *Frontiers in Genetics* 13 (2022): 994003.

Supporting Information

Additional supporting information can be found online in the Supporting Information section.